cyclic hemiacetal form (3, 27). Because the cyclic hemiacetal form of HNE is relatively stable (5), the detection of HNE Michael adduct is considered a reliable index of lipid peroxidation. This property enabled us to measure HNE-histidine Michael adduct using the specific antibody to cyclic hemiacetal type of HNE-histidine Michael adduct.

To clarify the influence of lipid peroxidation on the pathogenesis of AD, we directly assessed the cyclic hemiacetal type of HNE-histidine Michael adduct in brain specimens from AD subjects and age-matched controls. As a result, the HNE adduct was detected in the hippocampi of both groups, especially the CA2, CA3 and CA4 sectors. The important difference was significantly higher levels of the HNE adduct in the brains of patients with AD. This is the first report of specific antibody usage for direct detection of HNE-histidine Michael adduct in the cyclic hemiacetal form within hippocampi from humans with AD.

MATERIALS AND METHODS

Human subjects.

All clinical data from patients and information at autopsies from four patients with AD (two women and two men) and four (one women and three men) normal (no AD), age-matched subjects who died during the last several decades were retrieved from the autopsy database of the Department of Tokyo Metropolitan Geriatric Hospital, Tokyo, Japan. Brain specimens were registered in the Brain Bank for Aging Research (BBAR) organized by Tokyo Metropolitan Geriatric Hospital and Tokyo Metropolitan Institute of Gerontology (TMIG). Brain specimens used in this study were from patients clinically diagnosed as having AD-positive and control subjects without any sign of AD. All AD patients met accepted criteria for the neuropathologic diagnosis of AD based on the National Institute of Aging (NIA)-Reagan Institute Criteria for the Neuropathological Diagnosis of AD (1997) (1), combining abundant neuritic plaques in the neocortex (definite AD with Consortium to Establish a Registry for AD criteria) and a profusion of NFTs in the limbic and neocortical areas (Braak and Braak staging, VI). Normal subjects used as controls were individuals with no history of dementia or other neurological disorders. Neuropathologic evaluation of control brains revealed only age-associated gross and histopathologic alterations (Braak and Braak NFT staging, I and SP stage, 0 or A). The subjects' demographic data are summarized in Table 1. The human studies were approved by Ethics Committees of TMIG and the Tokyo Metropolitan Geriatric Hospital.

Immunohistochemistry.

Specimens were taken from the hippocampus and fixed with 4% paraformaldehyde in this study. Paraffin-embedded hippocampal sections were deparaffinized, rehydrated with xylene, alcohol and phosphate buffered saline (PBS), microwaved for 5 min in boiling 10 mM citrate buffer, pH 6.0, and immersed in 3% H_2O_2 in methanol for 15 min to reduce endogenous peroxidase activity. After blocking treatment with 10% non-immune goat serum in PBS (blocking solution) for 60 min at room temperature, the specimens were incubated with the primary antibodies overnight at 4°C and then for 60 min at room temperature. Mouse

monoclonal antibody against HNE-histidine Michael adduct which specific for their cyclic hemiacetal form was purchased from NOF Corporation (Tokyo, Japan), and was used at a dilution of 1:100 with a blocking solution. After adequate washing with PBS, specimens were incubated with the secondary antibody (goat anti-mouse IgG conjugated with horseradish peroxidase, Simplestain MAX-PO (M), Nichirei Biosciences Inc., Tokyo, Japan) for 60 min at room temperature. Thorough washing with PBS and incubation with 0.02% 3,3'-diaminobenzidine tetrahydrochloride (DAB) (Wako Pure Chemical Industries, Osaka, Japan) followed for 10 min at room temperature to visualize HNE-adduct. For double-labeling immunohistochemistry, two primary antibodies were used: anti-microtubule-associated protein 2 (MAP2) and the anti-HNE-histidine adduct antibodies. Tissue specimens were incubated with the anti-MAP2 antibody (1:500 dilution, Chemicon AB5622, rabbit polyclonal antibody, Billerica, MA, USA) to confirm pyramidal neurons, and then with Simplestain AP (R) as a secondary antibody conjugated with alkaline phosphatase. The alkaline phosphatase activity was visualized with Vector Red Alkaline Phosphatase Substrate Kit I (Vector Laboratories, Burlingame, CA, USA). Subsequently, the specimens were incubated with the anti-HNE adduct antibody as mentioned above. Hematoxylin was used for counter staining. The antibody used against HNE-histidine Michael adduct is specific for their cyclic hemiacetal form and does not react with the ring-opened form of HNE-histidine Michael adduct and the pyrrole form of HNE-lysine Michael adduct (26).

The four hippocampal sectors (CA1 through CA4) were delineated and cells that had a large nucleus containing a clearly visible nucleolus in theses sectors were referred to pyramidal cells according to the description of Mani *et al.*(14). Immunoreactive intensity of the HNE-Michael adduct was assessed by measuring 20 fields of hippocampal sectors in the specimens under a 40× objective microscopic field. The extent of staining intensity in pyramidal cells was classified into the following two grades: Pyr-small (small staining size less than half of the pyramidal cell nucleus) and Pyr-large (large staining size more than half of the pyramidal cell nucleus). The extent of staining intensity in non-pyramidal cells was also classified into the following two grades: Non-small (small staining size less than the cell nuclei) and Non-large (large staining size more than the cell nuclei). The percent ratio of these grades in each sector was calculated by following formulation: percent of Pyr-small = (numbers of Pyr-small grade / (numbers of Pyr-small grade + Pyr-large grade)) × 100, percent

of Pyr-large = (numbers of Pyr-large grade / (numbers of Pyr-small grade + Pyr-large grade)) × 100, percent of Non-small = (numbers of Non-small grade / (numbers of Non-small grade + Non-large grade)) × 100, percent of Non-large = (numbers of Non-large grade / (numbers of Non-small grade + Non-large grade)) × 100.

Statistical analysis.

The results are expressed as mean ± SEM. Statistical analyses were conducted by using Graphpad Prism 4 software (version 4.0, Graphpad Software Inc., San Diego, CA, USA). Significance was defined as a P value less than 0.05.

RESULTS

Clinical features of subjects

The subjects' demographic data are summarized in Table 1. The mean ages of the AD group and the control group were 86 and 78 years, respectively, and there was no significant difference between these two groups (*t-test*, two-sided). Neither brain weight, gender, nor postmortem interval differed significantly between the two groups according to a *t-test* (two-sided), Fisher's exact test, or *t-test* (two-sided), respectively.

HNE Michael adduct in the hippocampi from AD patients and non-AD controls

HNE Michael adduct in the hippocampi was detected in all specimens from both AD and controls. Especially, CA2-4 sectors contained an abundance of the HNE adduct compared with the adjacent CA1 sector (Fig. 1B and Table 2).

HNE Michael adduct immunoreactivity was seen as intracellular accumulations within pyramidal cells in the hippocampi of AD and controls (indicated in brown in Fig. 1C and D). In addition to the criteria of pyramidal cells in Materials and Methods, pyramidal cells were also confirmed by anti-MAP2 antibody as shown in Fig. 1D. The HNE adduct seemed to be composed of a mass of granular substances localized in the perikarya of pyramidal cells in the hippocampus, especially at the CA2, CA3 and CA4 sectors (Fig. 1C and D). Notably, the staining intensity for HNE Michael adduct was far stronger in these sectors of the AD brain samples than in those of the controls (Table 2, Fisher's exact test: $P< 0.0001$). Similarly, the ratio of the severe grade indicated as Pyr-large was relatively higher in the CA2/3 and CA4 sectors of AD patients compared with controls (Fig. 2A).

Additionally, a large amount of amorphous HNE Michael adduct was seen around the nuclei of non-pyramidal cells other than the pyramidal cells in the hippocampus, and this material is referred to as non-pyramidal cell deposits (abbreviated as Non-small and Non-large in Fig. 1C). Numerous non-pyramidal cell deposits were found in the CA2, CA3 and CA4 sectors of the hippocampi from AD and controls (Table 2), but the staining intensity of these deposits again differed significantly in the two groups (Table 2, Fisher's exact test: $P< 0.02$). That is, the ratio of large amorphous deposits (Non-large grade in Table 2) to total deposits was relatively higher in these sectors of the AD tissue compared with that from age-matched controls (Fig. 2B).

DISCUSSION

Here, we found an intracellular accumulation of HNE-histidine Michael adduct in pyramidal cells of the hippocampus, most notably at the CA2, CA3 and CA4 sectors by using a specific antibody to cyclic hemiacetal type of HNE-histidine Michael adduct. This antibody does not react with the ring-opened form of HNE-histidine Michael adduct and the pyrrole form of HNE-lysine Michael adduct (26). Although the HNE adduct occupied hippocampi from both AD and age-matched, non-AD controls, significantly larger quantities of the HNE adduct were present in the CA2-4 sectors of AD patients than those of controls. These results show that pyramidal neurons in these sectors within hippocampi of persons with AD are prone to undergo lipid peroxidation. Consequently, increased lipid peroxidation might be responsible for the neuronal degeneration and death characteristic of AD. In support is the fact that HNE, a lipid peroxidation product is cytotoxic to cultured neuronal cells via impairment of Na^+, K^+-ATPase (15), disruptions of microtubule structure (7, 20), caspase-3 activation, and cytochrome c release (6).

The distribution of the HNE adduct differed among CA sectors in the hippocampus. Although a few pyramidal cells in the CA1 sector contained the HNE adduct, a great number of cells in the CA2-4 sectors contained massive amounts of the HNE adduct. A similar spatial distribution pattern was found for malondialdehyde-conjugated proteins identified in persons with AD and age-matched controls (4). Thus, these results suggest that pyramidal cells in the CA1 sector might resist lipid peroxidation. On the other hand, after sodium borohydride treatment, the ring-opened form of HNE-histidine Michael adduct was seen frequently in hippocampi of AD patients but rarely in age-matched controls, and in the former case the percentage of immunoreactive pyramidal cells in the CA1 sector was comparable to that of the CA2-4 sectors (19). That result disagrees with the outcome presented here, possibly because antibodies of differing specificities were used in the two studies. That is, the previously used antibody against the ring-opened form of HNE-histidine Michael adduct rarely stained hippocampi from control subjects, whereas the antibody used in this study stained hippocampal tissues from controls and AD patients to comparable extents.

We also showed that amorphous deposits immunoreactive to the anti HNE adduct antibody in non-pyramidal cells were significantly increased in the CA2-4 sectors of hippocampal samples from AD patients compared with age-matched control. These deposits

were found around small nuclei in the CA2-4 sectors of hippocampal samples. Although the all cell types containing these small nuclei were not identified, some cells were positively stained with glial fibrillary acidic protein which is an astrocyte marker protein but not all cells. Immunoreactivity similar to the amorphous staining described here was seen in astrocytes when using antibody against the ring-opened form of HNE-histidine Michael adduct (19) and antibody against malondialdehyde-conjugated proteins (4). Therefore, the cells containing the small nuclei we viewed around amorphous deposits could be astrocytes.

In addition to the cyclic hemiacetal form and the ring-opened form of HNE-histidine Michael adduct, the pyrrole form of HNE-lysine Michael adduct (18, 24) was detected in the hippocampus (24) and entorhinal cortex (18) of samples from AD patients by using specific antibodies. Other than the immunohistochemical detection of HNE-conjugated proteins, elevated levels of HNE itself (17, 28) and isoprostanes (16, 22, 23), stable products derived from lipid peroxidation of PUFAs, these reports confirm increased lipid peroxidation in the brains of AD compared with control individuals. Thus, our results and those studies provide firm evidence of increased lipid peroxidation in brains that manifest AD.

Here we have documented strong evidence of lipid peroxidation in the hippocampi of both AD patients and age-matched, non-AD controls by identifying the presence of the HNE adduct. Presumably, the increased levels of HNE adduct in the hippocampi of AD patients signifies that the brains of such patients with AD tend to be more sensitive to lipid peroxidation than normal brains. In that environment, accelerated lipid peroxidation might play a pivotal role in the pathogenesis of AD by producing HNE and/or other cytotoxic products.

Acknowledgements

This study is supported by a Grant-in-Aid for Scientific Research from the Ministry of Education, Science, and Culture, Japan (to A.I., S.H. and N.S.) and a grant from Health Science Research Grants for Comprehensive Research on Aging and Health supported by the Ministry of Health Labor and Welfare, Japan (to A.I.). We thank Ms. Eiko Moriizumi for her technical advices on immunohistochemistry. We also thank Ms. P. Minick for the excellent English editorial assistance.

REFERENCES

1. (1997) Consensus recommendations for the postmortem diagnosis of Alzheimer's disease. The National Institute on Aging, and Reagan Institute Working Group on Diagnostic Criteria for the Neuropathological Assessment of Alzheimer's Disease. *Neurobiol. Aging* **18,** S1-2.
2. Abdul HM, Butterfield DA (2007) Involvement of PI3K/PKG/ERK1/2 signaling pathways in cortical neurons to trigger protection by cotreatment of acetyl-L-carnitine and alpha-lipoic acid against HNE-mediated oxidative stress and neurotoxicity: implications for Alzheimer's disease. *Free Radic Biol Med* **42,** 371-384.
3. Amarnath V, Valentine WM, Montine TJ, Patterson WH, Amarnath K, Bassett CN, Graham DG (1998) Reactions of 4-hydroxy-2(E)-nonenal and related aldehydes with proteins studied by carbon-13 nuclear magnetic resonance spectroscopy. *Chem Res Toxicol* **11,** 317-328.
4. Dei R, Takeda A, Niwa H, Li M, Nakagomi Y, Watanabe M, Inagaki T, Washimi Y, Yasuda Y, Horie K, Miyata T, Sobue G (2002) Lipid peroxidation and advanced glycation end products in the brain in normal aging and in Alzheimer's disease. *Acta Neuropathol* **104,** 113-122.
5. Esterbauer H, Schaur RJ, Zollner H (1991) Chemistry and biochemistry of 4-hydroxynonenal, malonaldehyde and related aldehydes. *Free Radic Biol Med* **11,** 81-128.
6. Ji C, Amarnath V, Pietenpol JA, Marnett LJ (2001) 4-hydroxynonenal induces apoptosis via caspase-3 activation and cytochrome c release. *Chem Res Toxicol* **14,** 1090-1096.
7. Kokubo J, Nagatani N, Hiroki K, Kuroiwa K, Watanabe N, Arai T (2008) Mechanism of destruction of microtubule structures by 4-hydroxy-2-nonenal. *Cell Struct Funct* **33,** 51-59.
8. Kruman I, Bruce-Keller AJ, Bredesen D, Waeg G, Mattson MP (1997) Evidence that 4-hydroxynonenal mediates oxidative stress-induced neuronal apoptosis. *J Neurosci* **17,** 5089-5100.
9. Liu X, Lovell MA, Lynn BC (2005) Development of a method for quantification of acrolein-deoxyguanosine adducts in DNA using isotope dilution-capillary LC/MS/MS

and its application to human brain tissue. *Anal Chem* **77,** 5982-5989.

10. Lovell MA, Ehmann WD, Butler SM, Markesbery WR (1995) Elevated thiobarbituric acid-reactive substances and antioxidant enzyme activity in the brain in Alzheimer's disease. *Neurology* **45,** 1594-1601.
11. Lovell MA, Markesbery WR (2007) Oxidative damage in mild cognitive impairment and early Alzheimer's disease. *J Neurosci Res* **85,** 3036-3040.
12. Lovell MA, Xie C, Markesbery WR (2001) Acrolein is increased in Alzheimer's disease brain and is toxic to primary hippocampal cultures. *Neurobiol Aging* **22,** 187-194.
13. Mamelak M (2007) Alzheimer' s disease, oxidative stress and gammahydroxybutyrate. *Neurobiol Aging* **28,** 1340-1360.
14. Mani RB, Lohr JB, Jeste DV (1986) Hippocampal pyramidal cells and aging in the human: a quantitative study of neuronal loss in sectors CA1 to CA4. *Exp Neurol* **94,** 29-40.
15. Mark RJ, Lovell MA, Markesbery WR, Uchida K, Mattson MP (1997) A role for 4-hydroxynonenal, an aldehydic product of lipid peroxidation, in disruption of ion homeostasis and neuronal death induced by amyloid beta-peptide. *J Neurochem* **68,** 255-264.
16. Markesbery WR, Kryscio RJ, Lovell MA, Morrow JD (2005) Lipid peroxidation is an early event in the brain in amnestic mild cognitive impairment. *Ann Neurol* **58,** 730-735.
17. Markesbery WR, Lovell MA (1998) Four-hydroxynonenal, a product of lipid peroxidation, is increased in the brain in Alzheimer's disease. *Neurobiol Aging* **19,** 33-36.
18. Montine KS, Olson SJ, Amarnath V, Whetsell WO, Jr., Graham DG, Montine TJ (1997) Immunohistochemical detection of 4-hydroxy-2-nonenal adducts in Alzheimer's disease is associated with inheritance of APOE4. *Am J Pathol* **150,** 437-443.
19. Montine KS, Reich E, Neely MD, Sidell KR, Olson SJ, Markesbery WR, Montine TJ (1998) Distribution of reducible 4-hydroxynonenal adduct immunoreactivity in Alzheimer disease is associated with APOE genotype. *J Neuropathol Exp Neurol* **57,**

415-425.

20. Neely MD, Sidell KR, Graham DG, Montine TJ (1999) The lipid peroxidation product 4-hydroxynonenal inhibits neurite outgrowth, disrupts neuronal microtubules, and modifies cellular tubulin. *J Neurochem* **72,** 2323-2333.

21. Porter NA, Caldwell SE, Mills KA (1995) Mechanisms of free radical oxidation of unsaturated lipids. *Lipids* **30,** 277-290.

22. Pratico D, V MYL, Trojanowski JQ, Rokach J, Fitzgerald GA (1998) Increased F2-isoprostanes in Alzheimer's disease: evidence for enhanced lipid peroxidation in vivo. *FASEB J* **12,** 1777-1783.

23. Reich EE, Markesbery WR, Roberts LJ, 2nd, Swift LL, Morrow JD, Montine TJ (2001) Brain regional quantification of F-ring and D-/E-ring isoprostanes and neuroprostanes in Alzheimer's disease. *Am J Pathol* **158,** 293-297.

24. Sayre LM, Zelasko DA, Harris PL, Perry G, Salomon RG, Smith MA (1997) 4-Hydroxynonenal-derived advanced lipid peroxidation end products are increased in Alzheimer's disease. *J Neurochem* **68,** 2092-2097.

25. Smith MA (1998) Alzheimer disease. *Int Rev Neurobiol* **42,** 1-54.

26. Tanaka T, Nishiyama Y, Okada K, Hirota K, Matsui M, Yodoi J, Hiai H, Toyokuni S (1997) Induction and nuclear translocation of thioredoxin by oxidative damage in the mouse kidney: independence of tubular necrosis and sulfhydryl depletion. *Lab Invest* **77,** 145-155.

27. Uchida K, Stadtman ER (1992) Modification of histidine residues in proteins by reaction with 4-hydroxynonenal. *Proc Natl Acad Sci U S A* **89,** 4544-4548.

28. Williams TI, Lynn BC, Markesbery WR, Lovell MA (2006) Increased levels of 4-hydroxynonenal and acrolein, neurotoxic markers of lipid peroxidation, in the brain in Mild Cognitive Impairment and early Alzheimer's disease. *Neurobiol Aging* **27,** 1094-1099.

29. Xiao Y, Huang Y, Chen ZY (2005) Distribution, depletion and recovery of docosahexaenoic acid are region-specific in rat brain. *Br J Nutr* **94,** 544-550.

FIGURE LEGENDS

Fig. 1 Representative photomicrographs of immunostaining for HNE-Michael adduct in the hippocampus. HNE-Michael adduct in the hippocampi of AD (A, C, D) and non-AD control (B) and MAP2 (D) are visualized using DAB (brown) and Vector Red (pink), respectively. Counter staining was performed with hematoxylin. Substances with immunoreactivity to anti-HNE-histidine Michael adduct are seen in pyramidal cells as a granular form (C, D) and seen in non-pyramidal cells as amorphous deposits (C). For statistical analysis, the extent of staining intensity of the HNE adduct is classified into two grades (Pyr-small and Pyr-large) for the pyramidal cells, and two grades (Non-small and Non-large) for the non-pyramidal cells, as described in Materials and Methods. Bar = 50 μm (A and B) and 5 μm (C and D).

Fig. 2 Ratio of immunostaining intensity of the HNE-Michael adduct in the hippocampal sectors. Immunostaining intensity of the HNE-Michael adduct was assessed as described in Materials and Methods. Percent of the grades of HNE staining intensity in each sector was calculated as described in Materials and Methods. (A), pyramidal cells; (B), non-pyramidal cells; closed bars, AD; open bars, age-matched controls. The percent ratio of the Pyr-large grade of the pyramidal cells and the percent ratio of the Non-large grade of the non-pyramidal cells are relatively higher in the CA2/3 and CA4 sectors of AD patients compared with controls.

Table 1 *Demographic data for AD subjects and controls*

	Age (yr)	PMI (h)	Gender	BW (g)	Braak stage	
					NFT	SP
AD	86 ± 3	10.0 ± 0.1	2 M/2 F	1,110 ± 52	VI (4)	C (4)
Controls	78 ± 2	4.4 ± 2.5	3 M/1 F	1,241 ± 67	I (4)	0 (4)

Data are expressed as mean ± SEM. Parentheses indicate the number of subject.

Abbreviations: AD, Alzheimer disease; PMI, postmortem interval; h, hour; BW, brain weight; g, gram; yr, year; NFT, neurofibrillary tangle; SP, senile plaque

Table 2 *Immunostaining intensity of the HNE-Michael adduct in the hippocampus*

		Pyramidal cells			Non-pyramidal cells		
Sector	Case	Pyr-small	Pyr-large	*P* value	Non-small	Non-large	*P* value
CA1	AD	228	39		126	95	
	Control	433	25	< 0.0001	143	125	NS
CA2/3	AD	168	433		236	463	
	Control	296	425	< 0.0001	177	255	0.0157
CA4	AD	42	238		177	299	
	Control	206	364	< 0.0001	205	223	0.0012

Staining intensity of the HNE adduct is classified into two grades (Pyr-small and Pyr-large) for the pyramidal cells, and two grades (Non-small and Non-large) for the non-pyramidal cells, as described in Materials and Methods.

Fisher's exact test; NS, not significant.

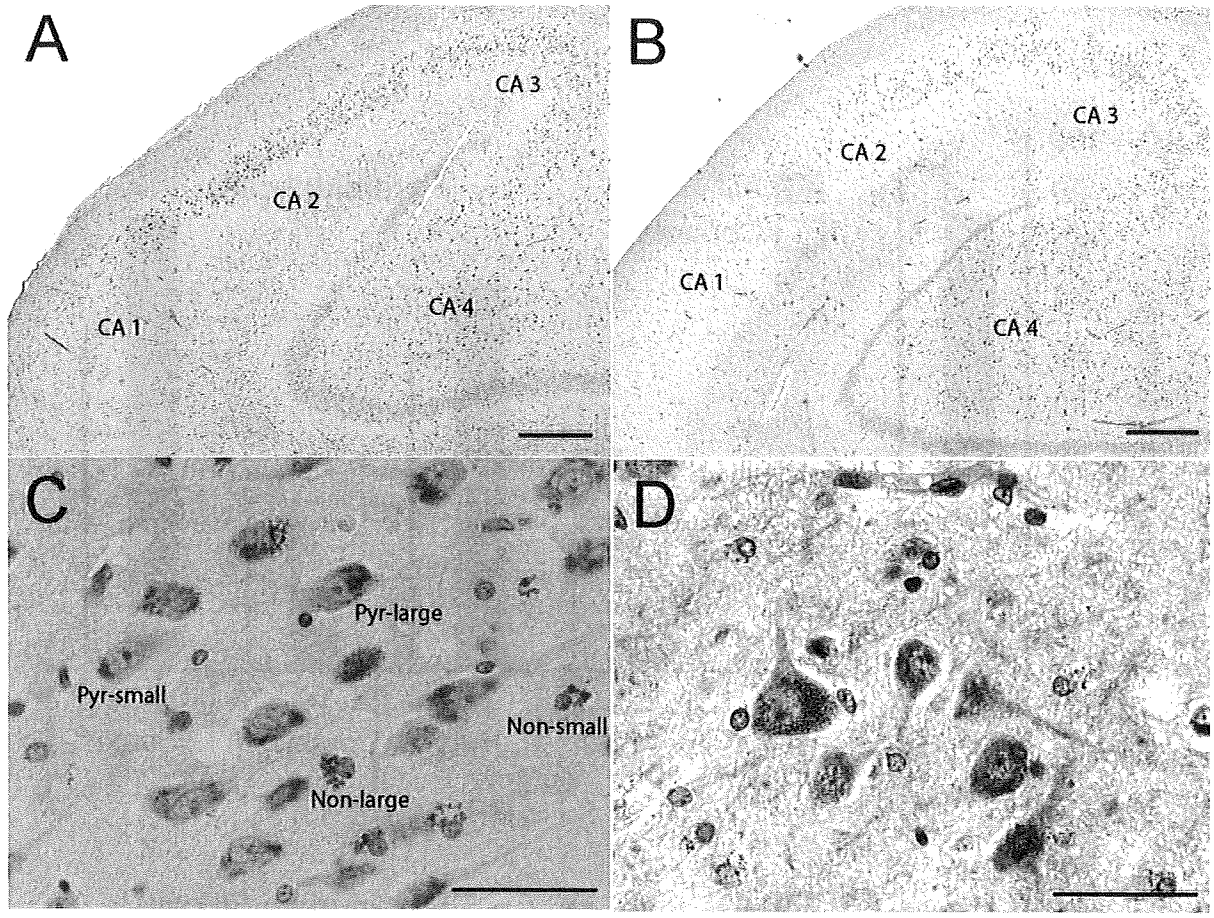
A
CA 3
CA 2
CA 4
CA 1
B
CA 3
CA 2
CA 1
CA 4
C
Pyr-large
Pyr-small
Non-small
Non-large
D

Figure 1

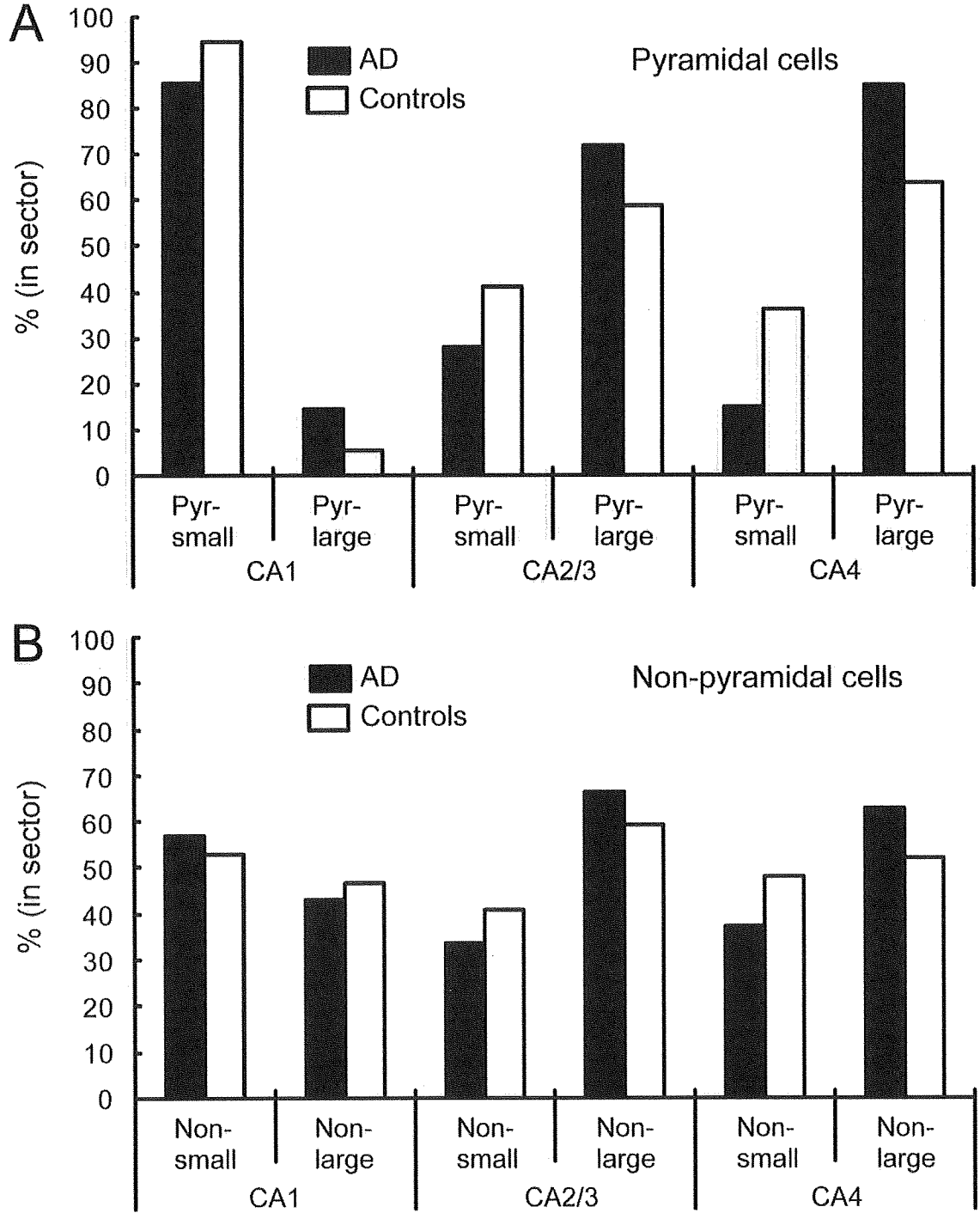
A
100
90
80
70
60
50
40
30
20
10
0
% (in sector)
AD
Controls
Pyramidal cells
Pyr-small
Pyr-large
Pyr-small
Pyr-large
Pyr-small
Pyr-large
CA1
CA2/3
CA4
B
100
90
80
70
60
50
40
30
20
10
0
% (in sector)
AD
Controls
Non-pyramidal cells
Non-small
Non-large
Non-small
Non-large
Non-small
Non-large
CA1
CA2/3
CA4

Figure 2

ORIGINAL RESEARCH

A.M. Tokumaru
Y. Saito
S. Murayama
K. Kazutomi
Y. Sakiyama
M. Toyoda
M. Yamakawa
H. Terada

Imaging-Pathologic Correlation in Corticobasal Degeneration

BACKGROUND AND PURPOSE: The clinical diagnosis of corticobasal degeneration (CBD) is often difficult due to varied clinical manifestations. In 4 patients with neuropathologically confirmed CBD, characteristic imaging findings and correlations with neuropathologic features were evaluated. Furthermore, imaging findings in CBD were compared with neuropathologically confirmed progressive supranuclear palsy (PSP) for a differential diagnosis.

MATERIALS AND METHODS: Four patients with neuropathologically confirmed CBD were studied. We evaluated the area of the tegmentum in the midsagittal plane, subcortical white matter (SCWM) abnormality, asymmetric cerebral atrophy, and signal-intensity abnormality in the subthalamic nuclei on MR imaging and compared them with histopathologic findings. Then, MR imaging findings in CBD were compared with those in 13 patients with PSP.

RESULTS: On MR imaging, 3 patients had asymmetric cerebral atrophy extending to the central sulcus. On midsagittal sections, the mean midbrain tegmentum area was 66 mm^2, being markedly smaller than normal, but there was no significant difference between PSP and CBD. All patients had signal-intensity abnormalities of the SCWM, constituting primary degeneration neuropathologically; however, no diffuse signal-intensity abnormality in the SCWM existed in the 13 patients with PSP. In 3 patients, T1-weighted images showed symmetric high signal intensity in the subthalamic nuclei. Neuropathologically, these areas showed characteristic CBD. MR imaging signal-intensity changes also existed in 4 patients with PSP; however, subthalamic nucleus degeneration was more severe in PSP than in CBD.

CONCLUSIONS: In cases with midbrain tegmentum atrophy and signal-intensity changes in the subthalamic nuclei, the differential diagnosis distinguishing CBD from PSP based on MR imaging alone was difficult. White matter lesions and asymmetric atrophy can be useful for a differential diagnosis.

Corticobasal degeneration (CBD) is a slowly progressive disorder with a clinically asymmetric onset characterized by apraxia, dystonia, postural instability, and an akinetic-rigid syndrome that does not respond to levodopa. However, clinical phenotypes of Alzheimer disease, Pick disease, and progressive supranuclear palsy (PSP) with similar characteristic features often make a differential diagnosis distinguishing these entities from CBD difficult in clinical practice.

Koyama et al[1] recently reported asymmetric cerebral atrophy with dominance contralateral to the more clinically affected side, hyperintensity in the subcortical white matter (SCWM) in the frontotemporal area on fluid-attenuated inversion recovery (FLAIR), and atrophy of the midbrain tegmentum as new imaging findings of clinically diagnosed CBD, but no imaging findings in pathologically proved cases have been reported.[3,4] We encountered 4 patients with neuropathologically confirmed CBD in whom the findings could be compared with those of MR imaging. Cortical symptoms were unclear in 3, and it was difficult to make a diagnosis on the basis of clinical symptoms alone because of underlying dementia. Although the number of cases was small, because the neuropathology and images were collated in all cases, this study was significant with regard to the objectivity of the imaging findings associated with an accurate diagnosis. We also thought that it was important to identify differences in imaging findings between CBD and PSP, in which severe atrophy of the midbrain tegmentum has been reported.[1,2] Therefore, MR imaging findings in CBD were compared with those in 13 cases of neuropathologically confirmed PSP.

Received January 3, 2009; accepted after revision May 12.

From the Departments of Diagnostic Radiology (A.M.T., M.T., M.Y.), Neuropathology (S.M.), and Neurology (K.K.), Tokyo Metropolitan Medical Center of Gerontology, Itabashi-Ku, Tokyo, Japan; Department of Neuropathology (Y. Saito), National Center of Neurology and Psychiatry, Kodaira, Tokyo, Japan; Department of Neurology (Y. Sakiyama), Jichi Medical College, Omiya, Saitama, Japan; and Department of Radiology (H.T.), Toho University, Sakura Medical Center, Sakura, Chiba, Japan.

Please address correspondence to Aya M. Tokumaru, MD, PhD, Department of Radiology, Tokyo Metropolitan Medical Center of Gerontology, 35-2 Sakaecho, Itabashi-ku, Tokyo 173-0015, Japan; e-mail: tokumaru@tmghig.jp

DOI 10.3174/ajnr.A1721

Materials and Methods

Patients

Four patients (1 man, 3 women) with neuropathologically confirmed CBD were evaluated retrospectively. The patients' mean age at death was 70.8 years (range, 67–74 years). Table 1 lists the patient characteristics. The MR imaging findings in the patients with CBD (Table 2) were compared with those in 13 patients with neuropathologically confirmed PSP. All 13 patients with PSP were men, with a mean age at death of 78.3 years (range, 64–87 years). For the comparative evaluation of atrophy of the midbrain tegmentum, 10 aged-matched control subjects (4 men and 6 women) with no neuropathologic degenerative disease or cerebrovascular disorder were selected (mean age at death, 74.6 years; range, 68–83 years).

MR Imaging Examinations

All studies were performed with a 1.5T MR imaging unit (Signa Excite HD; GE Healthcare, Milwaukee, Wis). Axial T2-weighted images (TR/TE, 4300/89 ms; NEX, 2; FOV, 220 mm; section thickness, 5 mm with a section gap of 1 mm) and FLAIR images (TR/TE, 10,002/106 ms; TI, 2500 ms; NEX, 1; section thickness, 5 mm with a gap of 1 mm), sagittal T1-weighted images (TR/TE, 600/14 ms; NEX, 2; section thickness, 5 mm with a gap of 1 mm), or sagittal spoiled gradient-echo

Table 1: Clinical findings of pathologically confirmed corticobasal degeneration

Case No.	Age at Onset (yr)	Sex	Duration (yr)	Rigidity	Dystonia	Pyramidal Signs	Cortical Dysfunction	Vertical Gaze Palsy	Dementia	CDx
1	74	F	10	Lt>Rt	–	–	Ocular apraxia	+	Mute	PSP?
2	68	F	6	Lt>Rt			Apraxia (Lt hand)	±	+ Severe akinetic mute	AD
3	67	M	3	Rt>Lt			No cortical sign	+	+ Severe	PDD
4	74	F	6	Rt>Lt	–	–	–	+	+ Severe	CBD

Note:—CBD indicates corticobasal degeneration; PSP?, progressive supranuclear palsy suspected; CDx, clinical diagnosis; AD, Alzheimer disease; PDD, Parkinson disease with dementia; –, no symptom; +, obvious symptom; ±, suspicious symptom; Lt, left; Rt, right.

Table 2: MR imaging findings of neuropathologically confirmed corticobasal degeneration

Case No.	Atrophy (Dominant Cerebral Hemisphere)	White Matter Hyperintensity on FLAIR		Hyperintensity on T1WI in Bil Subthalamic Nucleus
		Precentral Gyrus	Frontal Lobe	
1	Rt frontal operculum and convexity	–	+	+
2	Bil frontal convexity	–	+	+
3	Lt frontoparietal	Bil	+	+
4	Rt frontoparietal	Rt	+	+

Note:—FLAIR indicates fluid-attenuated inversion recovery; T1WI = T1-weighted imaging; Bil, bilateral; –, no signal abnormality; +, obvious signal abnormality.

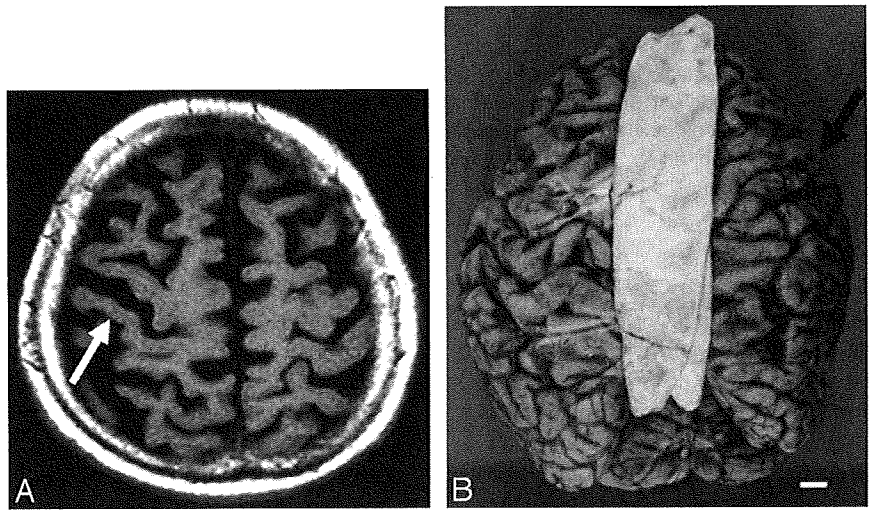

Fig 1. Corticobasal degeneration, case 1. An 84-year-old woman. *A*, Axial T2-weighted image shows right-side-dominant atrophy including the central sulcus (*arrow*). *B*, A macrospecimen of this patient shows right-frontal-dominant atrophy (*arrow*).

images (TR/TE, 21/6 ms; TI, 0 ms; flip angle, 20°) were obtained in all patients with CBD and PSP and healthy controls. Spin-echo coronal T1-weighted images (TR/TE, 600/14 ms; NEX, 2; section thickness, 5 mm with a gap of 1 mm) were obtained in 3 of the 4 patients with CBD, 7 of the 13 patients with PSP, and the 10 age-matched healthy controls. In 1 patient with CBD and 3 with PSP, T1-weighted coronal spin-echo images could not be obtained; spoiled gradient-echo imaging (TR/TE, 21/6 ms; TI, 0 ms; flip angle, 20°) was selected instead. These patients and 3 other patients with PSP without coronal sections were excluded from evaluation of the T1-weighted signal intensity. The area of the midbrain tegmentum was measured on an MR imaging workstation by using the method of Oba et al[2] in a T1-weighted midsagittal section through the center of the interpeduncular cistern and the center of the cerebral aqueduct. Two neuroradiologists (A.M.T. and M.T.) performed these measurements blindly, twice at different times.

The localization and laterality of cerebral atrophy, signal intensity in the subthalamic nuclei, and signals in the SCWM were only qualitatively investigated because of the limitations of the retrospective nature of pathologically confirmed cases. The 2 neuroradiologists blindly investigated images of 4 patients with CBD, 13 patients with PSP, and 10 healthy controls twice at different times and visually evaluated the following points: 1) the presence or absence and laterality of cerebral atrophy and whether the atrophy included the central sulcus on T1-weighted imaging, 2) the presence or absence and localization of a high signal intensity in the SCWM on T2-weighted or FLAIR imaging, and 3) the presence or absence of an increase in the signal intensity in the subthalamic nuclei in the coronary view on T1-weighted imaging.

Neuropathologic Examinations

Informed consent for autopsy was obtained from all of the patients or their families. All serial autopsy cases were examined with the Brain Bank Aging Research protocol, irrespective of clinical diagnosis.[3] At autopsy, after taking photographs of the whole brain, we serially sectioned the nondominant hemisphere or the hemisphere spared from focal lesions at a 7-mm thickness. The cerebrum was cut on the coronal plane; the brain stem, on the axial plane; and the cerebellum, on

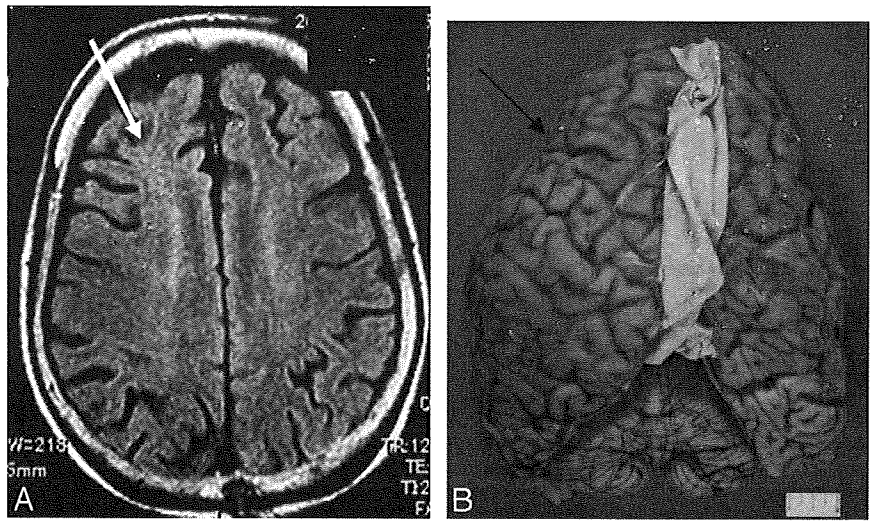

Fig 2. Corticobasal degeneration, case 2. A 74-year-old woman. *A*, An axial fluid-attenuated inversion recovery image 3 years before autopsy shows no obvious asymmetric atrophy. Subcortical hyperintensity is shown in the right frontal white matter (*white arrow*). *B*, A macrospecimen of this patient shows mild frontal atrophy with some asymmetry (*arrow*).

the sagittal plane. Photographs were taken of all sections. Small pieces of the anterior amygdala; posterior hippocampus; frontal, temporal, and occipital poles; supramarginal gyrus; and rostral midbrain were directly fixed in 4% paraformaldehyde for 48 hours and prepared for immunohistochemical and ultrastructural studies. The remaining sections were quick frozen and stored at −80°C. The hemisphere kept for morphologic examinations was fixed in 20% neutral buffered formalin for 7–13 days and cut into 7-mm-thick sections, similar to those in the contralateral hemisphere. Paraffin-embedded sections of representative areas of the brain were examined.

The selected anatomic structures included those recommended by the Consortium to Establish a Registry for Alzheimer Disease,[4] the Consensus Guidelines for the Diagnosis of Dementia with Lewy Bodies,[5,6] Braak and Braak's recommendation,[7] and the Diagnostic Criteria of Corticobasal Degeneration and Progressive Supranuclear Palsy.[8,9] These included the frontal pole; temporal pole; cingulate gyrus; second frontal gyrus; accumbens and septal nuclei; amygdala; basal nucleus of Meynert; second temporal gyrus; anterior hippocampus with entorhinal and transentorhinal cortices; basal ganglia and hypothalamus with mamillary bodies; subthalamic nucleus; posterior hippocampus; thalamus with the red nucleus; motor cortex; parietal lobe with the intraparietal sulcus; visual cortex; midbrain; upper and middle pons; medulla oblongata; cerebellar vermis; dentate nucleus; and multiple cervical, thoracic, and lumbar levels of the spinal cord.

Six-micrometer-thick sections were routinely stained with hematoxylin-eosin and the Klüver-Barrera method. Selected sections were stained with the modified methenamine, Gallyas-Braak, and Bielschowsky silver staining for age-related changes, with Congo red for amyloid β deposition and elastica-Masson trichrome staining for vascular changes.

Immunohistochemistry

Six-micrometer-thick serial sections were immunohistochemically stained by using a 20NX autostainer (Ventana, Tucson, Ariz), as previously described. The antibodies applied to all the cases were the following: antiphosphorylated α-synuclein (psyn); phosphorylated tau (ptau) (AT8, monoclonal; Innogenetic, Temse, Belgium); 3-repeat tau (RD3, amino acids 209–224, monoclonal, Upstate; Millipore, Lake Placid, NY); 4-repeat tau (RD4, amino acid 275–291, monoclonal, Upstate; Millipore); amyloid β 11–28 (12B2, monoclonal; IBL, Maebashi, Japan); glial fibrillary acidic protein (polyclonal; DAKO, Glostrup, Denmark); HLA-DR (monoclonal, CD68; DAKO); phosphorylated neurofilament (monoclonal SMI31; Sternberger Immunochemical, Baltimore, Md); myelin basic proteins (polyclonal, DAKO); and ubiquitin (polyclonal, DAKO) antibodies.

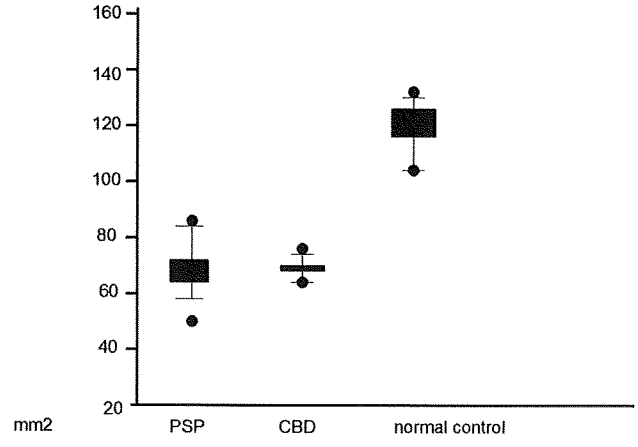

Fig 3. Scatterplot (mean, SD, and range) of the area of the midbrain in patients with progressive supranuclear palsy (PSP), corticobasal degeneration (CBD), and age-matched healthy controls. There was no individual overlap of the midbrain tegmental area between the healthy controls and patients with CBD and PSP, apparently showing that severe atrophy of the midbrain tegmentum was present in patients with CBD and PSP.

In addition to the routine neuropathologic examination mentioned above, studies were performed at sites of MR imaging signal-intensity abnormalities or atrophy to correlate the radiologic and pathologic findings. To compare them with MR imaging findings, 2 neuropathologists investigated the following points in addition to routine examinations: 1) the macroscopic presence or absence, laterality, and localization of cerebral atrophy at the time of sectioning the brain and after fixation, 2) the macroscopic presence or absence of atrophy of the midbrain tegmentum at the time of sectioning the brain and after fixation, 3) the presence or absence and degree of degeneration of the subthalamic nuclei, and 4) the presence or absence of a lesion in the SCWM and whether the lesion constituted primary or secondary degeneration in CBD. For brain samples, 7-mm coronal sections of the lateral region passing the mamillary body vertical to the hippocampal structure were prepared. Abnormal intensi-

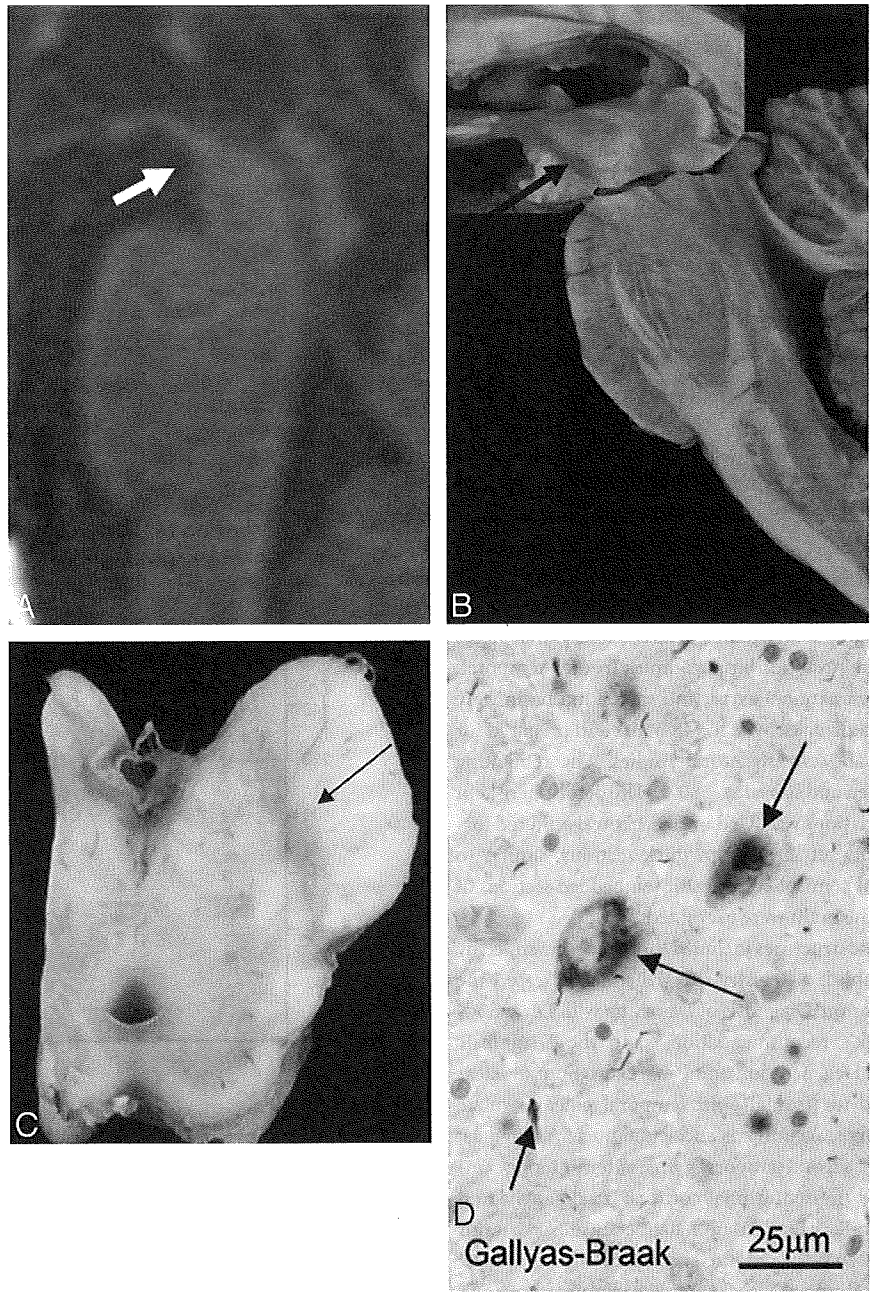

Fig 4. Corticobasal degeneration (CBD), case 1. An 84-year-old woman. *A*, T1-weighted midsagittal image clearly shows atrophy of the midbrain tegmentum (*arrow*). The area of the midbrain tegmentum is 73 mm^2. *B*, A macroscopic specimen of the midbrain shows marked atrophy (*arrow*). *C*, A macroscopic view of the midbrain shows discoloration of the substantia nigra (*arrow*). *D*, A microscopic view of the substantia nigra (Gallyas-Braak stain) shows argyrophilic threads and granular or fibrous inclusion bodies (*arrows*). These are consistent with CBD.

ties on MR imaging were collated with the pathologic preparations as accurately as possible, with the line passing the mamillary body vertical to the hippocampal structure as the baseline, and new pathologic sections were cut out as needed.

Results

Asymmetric Cerebral Atrophy

Asymmetric cerebral atrophy was observed in 3 of 4 patients with predominance contralateral to the more clinically affected side. In all 3 patients, cerebral atrophy affected the area including the central sulcus. In 1 patient, the radiologic and pathologic findings of predominantly frontal lobe atrophy were correlated (case 1, Fig 1*A*, -*B*). In 1 patient (case 2, Fig 2*A*, -*B*) in whom the interval between MR imaging and autopsy was 3 years, asymmetric cortical atrophy was difficult to detect on MR imaging, but frontal atrophy with some asymmetry was seen on autopsy. In this patient, clinical evaluation revealed no asymmetric cortical symptoms, so the clinical diagnosis was Alzheimer disease. In the 13 cases with PSP, excluding 1 patient, no asymmetric atrophy was noted.

Atrophy of Midbrain Tegmentum

On midsagittal sections, by using the method of Oba et al,[2] the mean area of the midbrain tegmentum of the 4 patients with CBD was 67.6 ± 7.4 mm^2 (range, 62.3–73.3 mm^2) (Fig 3; case 1, Fig 4*A*–*D*), which is markedly less than normal, with the

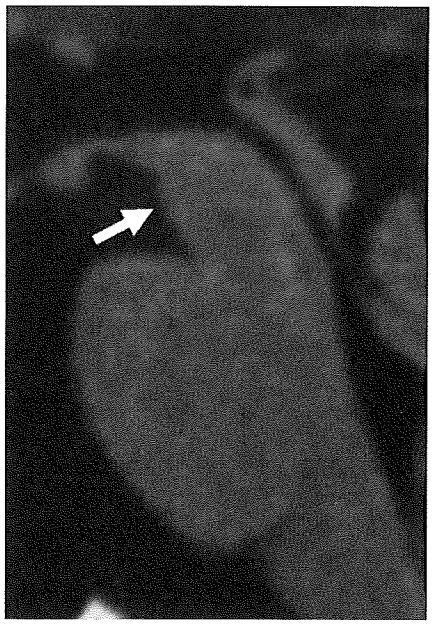

Fig 5. An age-matched healthy control 72-year-old woman. T1-weighted midsagittal image shows no obvious atrophy of the midbrain tegmentum (*arrow*). The area of the midbrain tegmentum is 128 mm^2.

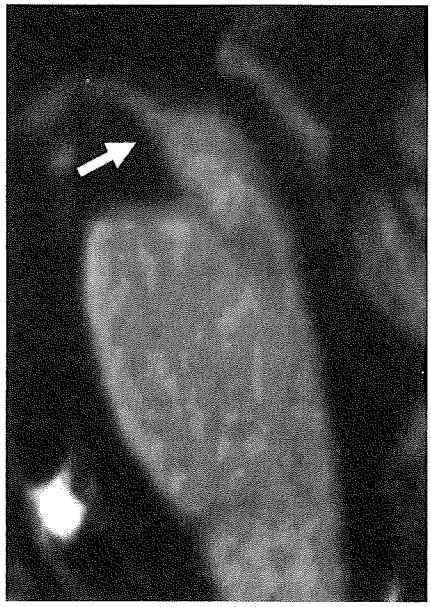

Fig 6. Progressive supranuclear palsy. A 74-year-old man. T1-weighted midsagittal image clearly shows atrophy of the midbrain tegmentum (*arrow*). The area of the midbrain tegmentum is 71 mm^2.

mean area of 123.8 ± 10.8 mm^2 in the controls (range, 108.0–132.4 mm^2) (Figs 3 and 5). In the 13 patients with neuropathologically confirmed PSP, the mean area was 70.7 ± 12.1 mm^2 (range, 58.6–89.8 mm^2) (Figs 3 and 6). Although statistical analysis was not possible because of the small number of cases, there was no individual overlap of the midbrain tegmental area between the healthy controls and patients with CBD and PSP, apparently showing that severe atrophy of the midbrain tegmentum was present in CBD and PSP. On neuropathologic examination, there was also atrophy of the midbrain tegmentum and marked depigmentation of the substantia nigra and locus ceruleus. Other findings included melanophagia and gliosis, and Gallyas-Braak silver staining revealed argyrophilic threads and granular or fibrous inclusion bodies. These findings were consistent with CBD. In the pontine tegmentum and oculomotor and trochlear nuclei, many AT8-immunoreactive pretangles were observed.

SCWM Signa-Intensity Change on T2-Weighted Images and FLAIR

In all 4 patients with CBD, T2-weighted images and FLAIR showed diffuse high-intensity signals in the SCWM. In 3 patients, high signal intensity in the SCWM was recognized on the predominantly atrophic side (case 1, Fig 7*A*–*C*). In 1 patient, a high signal intensity was noted bilaterally over a wide area in the frontal lobes (case 3, Fig. 8*A*–*C*). Corresponding to the sites of white matter lesions, myelin sheath staining was decreased, and these sites were stained positively for antiphosphorylated tau antibody. These changes are primary characteristic of CBD. On neuropathologic examination, there was some involvement of U-fibers, but because of image-quality limitations on MR imaging, U-fiber involvement could not be specifically detected. In the 13 patients with PSP, there was no diffuse signal-intensity abnormality in the SCWM. There was no neuropathologic finding indicating primary degeneration of the SCWM.

Symmetric High Signal Intensity Bilaterally in Subthalamic Nuclei on T1-Weighted Images

T1-weighted MR images showed symmetric high signal intensity bilaterally in the subthalamic nuclei in all 3 patients in whom T1-weighted images were obtained (case 1, Fig 9*A*–*C*). In the remaining patient, the signal intensity in the subthalamic nuclei was not evaluated because no T1-weighted coronal spin-echo images could be obtained. Spoiled gradient echo (TR/TE, 21/6 ms; TI, 0 ms; flip angle, 20°) was selected instead. These sites showed a brownish change on macroscopic examination, and on microscopic examination, antiphosphorylated tau antibody–positive neurons and gliosis were observed. These changes were characteristic of CBD. MR imaging signal-intensity changes were also present in 4 of 7 patients with PSP in whom T1-weighted images were obtained (Fig 10*A*–*C*). Because neuropathologically examined cases were retrospectively evaluated, signal-intensity evaluation was limited to visual examination by 2 neuroradiologists. It was difficult to distinguish CBD and PSP on imaging, and no asymmetry was identified. However, on neuropathologic examination, degeneration of the subthalamic nuclei was more severe in PSP than in CBD.

Discussion

In 3 of the 4 patients with CBD, atrophy was predominantly contralateral and extended to the central sulcus. On neuropathologic examination, the MR imaging findings of atrophy were confirmed. In 1 patient with no asymmetric cortical symptoms, there was no asymmetry on MR imaging (case 2, Fig 3*A*, *-B*) and the clinical diagnosis was Alzheimer disease. In this patient, in whom the interval between the last MR imaging and autopsy was 3 years, neuropathologic examination did show asymmetric atrophy, but it was mild compared with that in the other 3 patients. In some patients, CBD presents with dementia, behavioral abnormalities, and attention deficit in

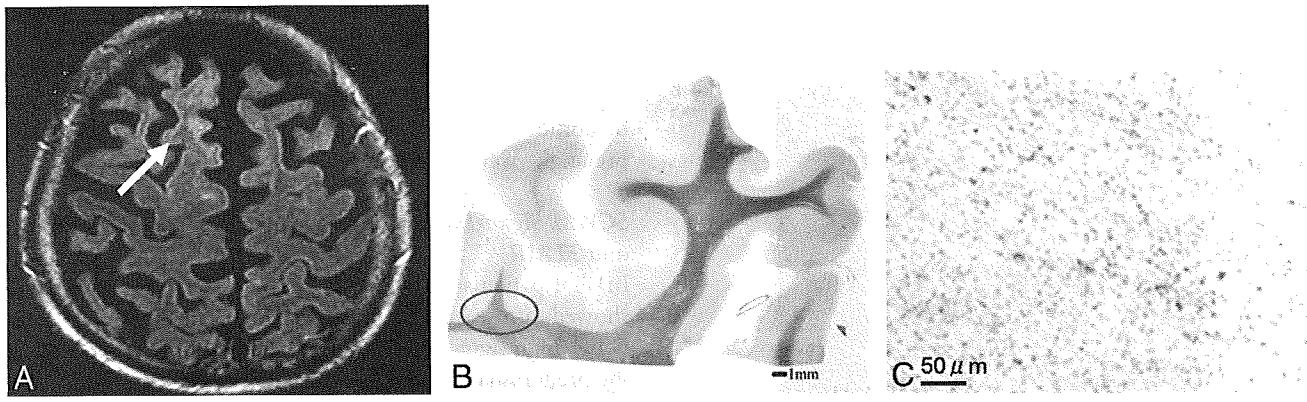

Fig 7. Corticobasal degeneration (CBD), case 1. An 84-year-old woman. *A*, Axial T2-weighted image shows a high signal intensity in the right frontal subcortical white matter (*white arrow*). *B*, In a microscopic specimen of the right frontal lobe corresponding to the site of white matter lesions, myelin sheath staining is decreased (*red oval*). The scale is 1 mm. *C*, In this area, there is positive staining for antiphosphorylated tau antibody on AT8 staining, which is compatible with the primary changes in CBD. The scale is 50 μm.

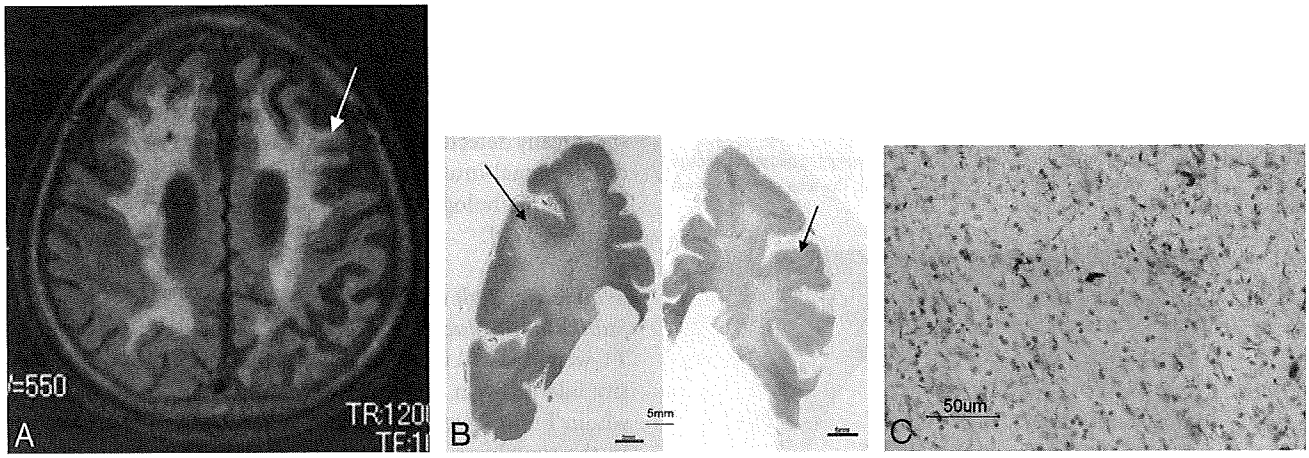

Fig 8. Corticobasal degeneration (CBD), case 3. A 70-year-old man. *A*, An axial fluid-attenuated inversion recovery image shows a high signal intensity bilaterally over a wide area in the frontal lobes (*arrow*). *B*, Corresponding to sites of white matter lesions, myelin sheath staining is decreased (*arrow*). The scale is 5 mm. *C*, These sites are stained positively for antiphosphorylated tau antibody. The scale is 50 μm. The changes are primary characteristics of CBD.

the early stage, but patients may be misdiagnosed due to a lack of cortical symptoms.[10-14] The above patient (case 2) may be an example of such a clinical presentation. Clinical evaluation showed little evidence of asymmetric cortical dysfunction, and neuropathology revealed only minimal cortical asymmetry. In this case, MR imaging showed a slight high signal intensity in the frontal SCWM; the midbrain tegmentum was severely atrophied, with an area of 71 mm^2; and T1-weighted imaging showed symmetric high-intensity signals in the subthalamic nucleus. Although a clear description is difficult on the basis of only 1 case, it was demonstrated by the pathologic findings that when identification of the cortical sign is difficult and unilateral atrophy is unclear on imaging, imaging findings, such as atrophy of the midbrain tegmentum, an abnormal signal intensity in the SCWM on FLAIR, or signal intensity changes in the subthalamic nuclei on T1-weighted imaging, may serve as supportive findings suggesting CBD.

CBD is important to differentiate from PSP. Oba et al[2] described a convenient and objective approach to diagnosing PSP based on midsagittal measurement of the midbrain tegmentum area. However, Koyama et al[1] also reported midbrain tegmentum atrophy in CBD. In our 4 cases of neuropathologically confirmed disease, severe midbrain tegmentum atrophy was also observed. Although there was a limited number of cases, because there was no individual overlap of the midbrain tegmental area between the healthy controls and patients with pathologically confirmed CBD and PSP, investigation of midbrain tegmental atrophy may have led to the diagnosis of CBD and PSP. Although no statistical analysis was performed because of the limited number of cases, it may be difficult to differentiate CBD from PSP on the basis of the presence of midbrain tegmental atrophy alone. A so-called "penguin sign" may be a distinguishing feature of PSP, but with severe midbrain tegmentum atrophy, both PSP and CBD must be considered. On neuropathology, there was marked depigmentation of the substantia nigra and locus ceruleus. Other findings included melanophagia and gliosis, and Gallyas-Braak silver staining revealed argyrophilic threads and granular or fibrous inclusion bodies. These findings were consistent with CBD as a cause of the atrophy. The degeneration of motor nerve nuclei, including the oculomotor and abducens nuclei, in the brain stem tegmentum was also noted, but no corresponding imaging findings were seen in the present study.

The localization of SCWM abnormalities, though different from those in previous reports,[1,15] was prominent in the present study. In CBD, Tokumaru et al,[15] Doi et al,[16] and Koyama et al[1] described predominantly unilateral SCWM abnormalities on T2-weighted imaging and FLAIR. In their re-